Speed Control of an Electrical Drive

Vitesse - Track A - Trinome 32

Jin DING
Carlos BENÍTEZ ROSETY
Marcos Ichiro SASAKI

TP Report
Control Theory

19/09/2025 - 22/10/2025

Abstract

Lorem ipsum dolor sit amet, consectetuer adipiscing elit. Ut purus elit, vestibulum ut, placerat ac, adipiscing vitae, felis. Curabitur dictum gravida mauris. Nam arcu libero, nonummy eget, consectetuer id, vulputate a, magna. Donec vehicula augue eu neque. Pellentesque habitant morbi tristique senectus et netus et malesuada fames ac turpis egestas. Mauris ut leo. Cras viverra metus rhoncus sem. Nulla et lectus vestibulum urna fringilla ultrices. Phasellus eu tellus sit amet tortor gravida placerat. Integer sapien est, iaculis in, pretium quis, viverra ac, nunc. Praesent eget sem vel leo ultrices bibendum. Aenean faucibus. Morbi dolor nulla, malesuada eu, pulvinar at, mollis ac, nulla. Curabitur auctor semper nulla. Donec varius orci eget risus. Duis nibh mi, congue eu, accumsan eleifend, sagittis quis, diam. Duis eget orci sit amet orci dignissim rutrum.

Nam dui ligula, fringilla a, euismod sodales, sollicitudin vel, wisi. Morbi auctor lorem non justo. Nam lacus libero, pretium at, lobortis vitae, ultricies et, tellus. Donec aliquet, tortor sed accumsan bibendum, erat ligula aliquet magna, vitae ornare odio metus a mi. Morbi ac orci et nisl hendrerit mollis. Suspendisse ut massa. Cras nec ante. Pellentesque a nulla. Cum sociis natoque penatibus et magnis dis parturient montes, nascetur ridiculus mus. Aliquam tincidunt urna. Nulla ullamcorper vestibulum turpis. Pellentesque cursus luctus mauris.

Contents

1 Identification of the System Parameters

1.1 Introduction

The objective of this practical work is to design and implement control strategies for the speed regulation of a direct current (DC) electrical drive system. Such systems are widely used in transportation, robotics, and industrial automation, where precise speed control ensures efficiency and reliability.

The study combines modeling, simulation, and experimentation. First, the electrical and mechanical parameters of the DC motor are identified using a platform composed of two coupled DC machines, sensors, and a DC/DC converter. Then, controllers are designed and validated in Matlab/Simulinkan inner current loop by pole placement and an outer speed loop using a linear quadratic (LQ) approach. Finally, the controllers are tested on the physical setup to compare real and simulated performances.

Part 1 focuses on parameter identification, determining key characteristics such as resistance, inductance, torque and voltage constants, friction coefficients, and inertia. These parameters provide the foundation for accurate modeling and effective control design in the subsequent stages.

The equations governing the DC motor system are as follows:

$$U_m(t) = R \cdot I(t) + L\frac{dI(t)}{dt} + E(t) \tag{1}$$

$$E(t) = K_e \cdot \Omega(t) \tag{2}$$

$$C_e(t) = K_c \cdot I(t) \tag{3}$$

$$C_e(t) = C_r(t) + C_s + f \cdot \Omega(t) + J\frac{d\Omega(t)}{dt} \tag{4}$$

where:

- R: armature resistance (Ω)
- L: armature inductance (H)
- E: counter-electromotive force of the motor (V)
- Ω: rotational speed of the rotor ($\text{rad} \cdot \text{s}^{-1}$)
- C_e: electromagnetic torque of the motor ($\text{N} \cdot \text{m}$)

- K_e: voltage constant ($\mathrm{V} \cdot \mathrm{s}$)
- K_c: torque constant ($\mathrm{N} \cdot \mathrm{m} \cdot \mathrm{A}^{-1}$)
- C_r: resistant torque ($\mathrm{N} \cdot \mathrm{m}$)
- C_s: Coulomb friction torque ($\mathrm{N} \cdot \mathrm{m}$)
- f: viscous friction coefficient ($\mathrm{N} \cdot \mathrm{m} \cdot \mathrm{s}$)
- J: moment of inertia of the shafts of the two machines ($\mathrm{kg} \cdot \mathrm{m}^2$)

1.2 Armature resistance and inductance: R and L

The armature resistance (R) and inductance (L) characterize the electrical behavior of the DC motors armature circuit. The resistance R represents the opposition to the flow of current in the winding, while the inductance L reflects the ability of the winding to store energy in its magnetic field. These parameters directly influence the transient response of the current when a voltage is applied to the motor.

To determine R and L, the rotor is kept stationary so that no back electromotive force (EMF) is generated. A step voltage $u_c(t)$ of 2.5 V is applied through the DC/DC converter, and the corresponding current response is observed in the Simulink oscilloscope. The experiment can be modeled as a simple first-order RL circuit governed by:

$$U_m(t) = RI(t) + L\frac{dI(t)}{dt}.$$

At steady state, the current reaches a constant value I_∞, allowing the armature resistance to be calculated as:

$$R = \frac{U_m}{I_\infty}.$$

The inductance L is obtained from the electrical time constant τ_e of the current response, given by:

$$\tau_e = \frac{L}{R} \quad \Longrightarrow \quad L = R \cdot \tau_e.$$

The measured quantities during the experiment are summarized in Table 1.

Table 1: Measured and calculated values for R and L

Quantity	**Symbol**	**Measured Value**	**Unit**
Applied voltage	V	6.5	V
Steady-state current	I	18.55	A
Electrical time constant	τ_e	0.025	s
Calculated resistance	R	0.3504	Ω
Calculated inductance	L	0.00876	H

Thus, from the steady-state and transient measurements, the armature resistance and inductance of the DC machine were found to be:

$$R = 0.3504\ \Omega, \qquad L = 0.00876\ \text{H}.$$

These values will be used in subsequent stages for the modeling and control design of the electrical drive system.

1.3 Voltage constant and torque constant: $K_e = K_c$

1.4 Coulomb friction torque and viscous friction coefficient: C_s and f

1.5 Moment of inertia of the system: J

2 Controller Design and Validation by Simulations

Quisque ullamcorper placerat ipsum. Cras nibh. Morbi vel justo vitae lacus tincidunt ultrices. Lorem ipsum dolor sit amet, consectetuer adipiscing elit. In hac habitasse platea dictumst. Integer tempus convallis augue. Etiam facilisis. Nunc elementum fermentum wisi. Aenean placerat. Ut imperdiet, enim sed gravida sollicitudin, felis odio placerat quam, ac pulvinar elit purus eget enim. Nunc vitae tortor. Proin tempus nibh sit amet nisl. Vivamus quis tortor vitae risus porta vehicula.

Fusce mauris. Vestibulum luctus nibh at lectus. Sed bibendum, nulla a faucibus semper, leo velit ultricies tellus, ac venenatis arcu wisi vel nisl. Vestibulum diam. Aliquam pellentesque, augue quis sagittis posuere, turpis lacus congue quam, in hendrerit risus eros eget felis. Maecenas eget erat in sapien mattis porttitor. Vestibulum porttitor. Nulla facilisi. Sed a turpis eu lacus commodo facilisis. Morbi fringilla, wisi in dignissim interdum, justo lectus sagittis dui, et vehicula libero dui cursus dui. Mauris tempor ligula sed lacus. Duis cursus enim ut augue. Cras ac magna. Cras nulla. Nulla egestas. Curabitur a leo. Quisque egestas wisi eget nunc. Nam feugiat lacus vel est. Curabitur consectetuer.

Suspendisse vel felis. Ut lorem lorem, interdum eu, tincidunt sit amet, laoreet vitae, arcu. Aenean faucibus pede eu ante. Praesent enim elit, rutrum at, molestie non, nonummy vel, nisl. Ut lectus eros, malesuada sit amet, fermentum eu, sodales cursus, magna. Donec eu purus. Quisque vehicula, urna sed ultricies auctor, pede lorem egestas dui, et convallis elit erat sed nulla. Donec luctus. Curabitur et nunc. Aliquam dolor odio, commodo pretium, ultricies non, pharetra in, velit. Integer arcu est, nonummy in, fermentum faucibus, egestas vel, odio.

3 Experimental Validation of the Controllers

This section reports the laboratory validation of the controllers designed in Part 2. Several Simulink configurations were used successively (current loop, speed loop, and finally the observer). Due to limited laboratory time, **only the final implementation corresponding to the observer (Part 3.3) was saved as a representative Simulink diagram**. However, **all measurement results** obtained at each step were recorded and are presented below to assess the performance of every loop. Earlier configurations for the current and speed control followed the same structure as the final one (inner current loop, outer speed loop, voltage saturation, and acquisition blocks).

Practical constraints. For hardware safety, the armature current was limited to 20 A, voltage commands were saturated at ± 9 V, and step amplitudes were increased gradually to avoid excessive mechanical stress and large current transients.

3.1 Current Regulation Experiment

The experimental results of the current control loop are shown in Figure 2. The upper plot displays the armature current (*courant*) and the lower plot shows the corresponding motor speed (*vitesse*). Several step changes were applied to the current reference, increasing successively from approximately 1 A to 2 A, 3 A and finally 10 A. The current follows the reference with a fast transient and negligible overshoot, demonstrating a well-tuned inner current loop. Small fluctuations in the measured signal are mainly due to sensor noise. The motor speed evolves consistently with the current variations, rising up to about 1000 rpm and then decreasing when the current is reduced or reversed. This confirms the expected electromechanical coupling between torque and speed. At the end of the experiment, both current and speed return smoothly to zero when the converter command is disabled.

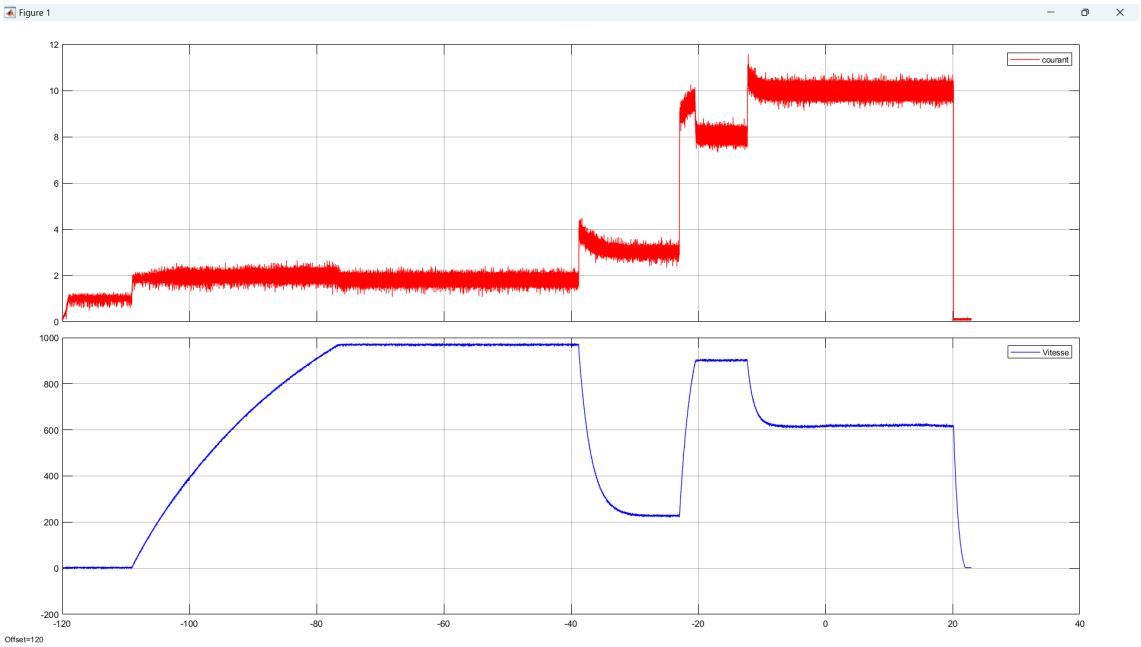

Figure 2: Measured current (top, in A) and speed (bottom, in rpm) during the current regulation test. The current loop shows fast and stable response with negligible overshoot.

3.2 Speed Regulation Experiment

The experimental validation of the speed controller was performed following the four test scenarios defined in Question 2.2.c. For each case, the converter operated in "Automatic" mode, and the speed reference $\Omega^*(t)$ was imposed through the control panel. The measured motor speed (*vitesse*) and armature current (*courant*) were recorded simultaneously.

- **Case 1** : $C_r(t) = 0$, $\Omega^*(t)$ changes from 0 to 300 rpm at $t = 1$ s.
- **Case 2** : $C_r(t) = 0$, $\Omega^*(t)$ changes from 0 to 500 rpm at $t = 1$ s.
- **Case 3** : $C_r(t) = 0$, $\Omega^*(t)$ changes from 0 to 1200 rpm at $t = 1$ s.
- **Case 4** : $\Omega^*(t)$ changes from 0 to 300 rpm at $t = 1$ s, while the resistant torque $C_r(t)$ increases from 0 to 5 Nm at $t = 10$ s.

The measured responses are summarized in Figures 3–6. In all cases, the speed regulation shows a well-damped transient with limited overshoot and negligible steady-state error. For moderate speed commands (300 rpm and 500 rpm), the current peaks remain within the admissible range (below 20 A), confirming that the current limiter effectively constrains the torque demand. When the reference is increased to 1200 rpm, the system still converges but the transient becomes slower, illustrating the saturation effect of the voltage converter.

When a disturbance torque of 5 Nm is applied at $t = 10$ s, a brief speed drop is observed, immediately compensated by the integral action of the speed controller. The steady-state speed returns to its nominal value within less than one second, demonstrating the robustness of the closed-loop regulation against load disturbances.

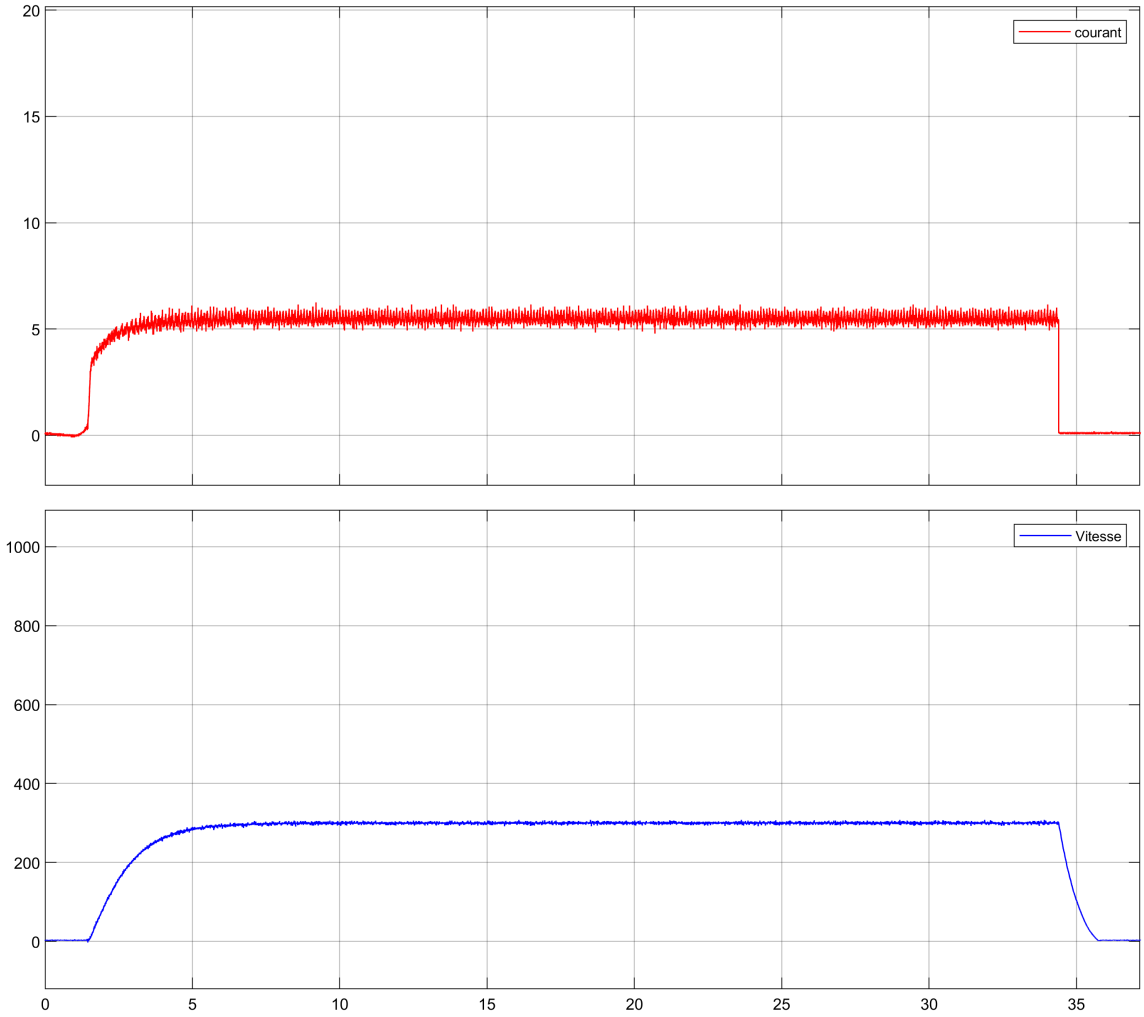

Figure 3: Speed loop — measured response for a $0 \rightarrow 300$ rpm reference step.

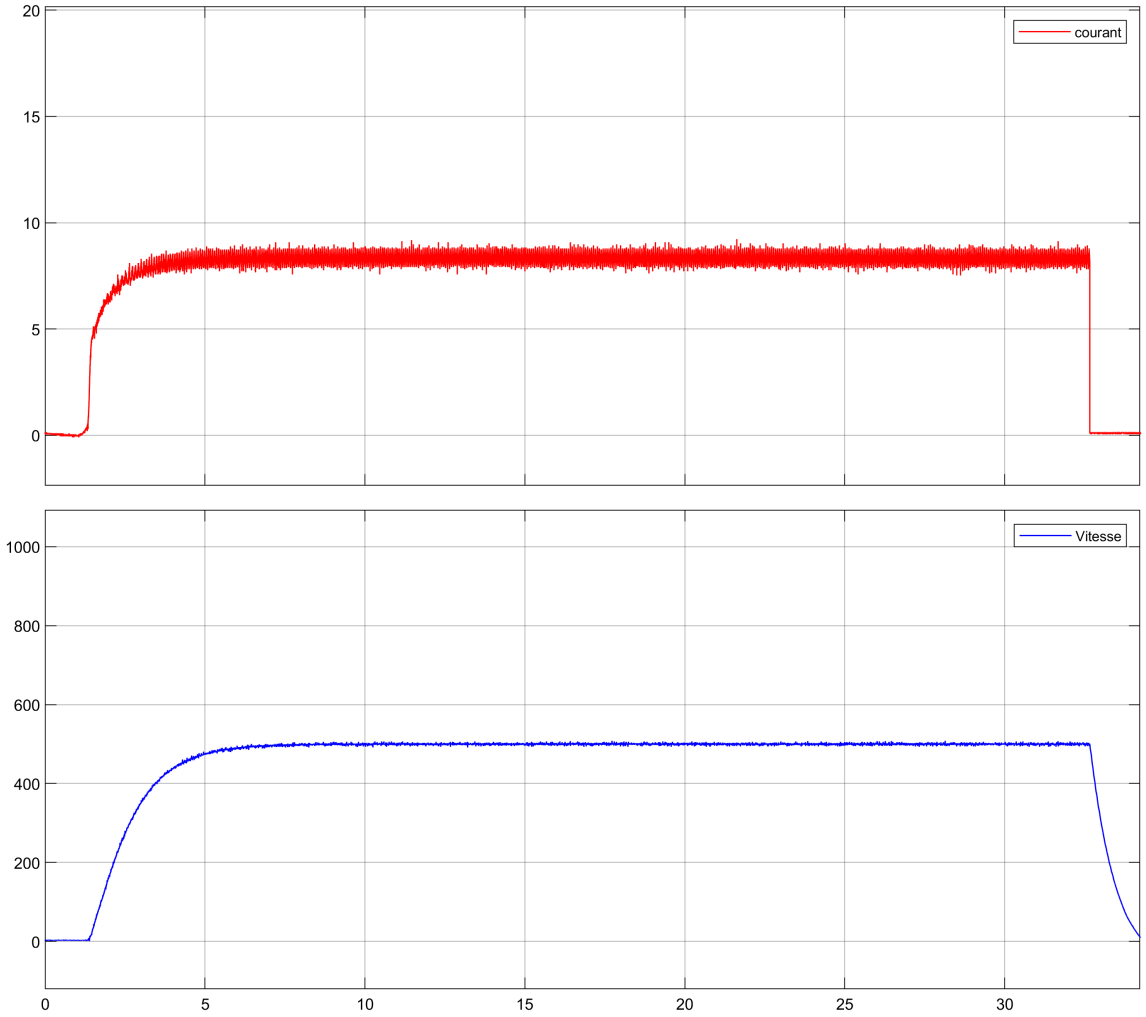

Figure 4: Speed loop — measured response for a $0 \rightarrow 500$ rpm reference step.

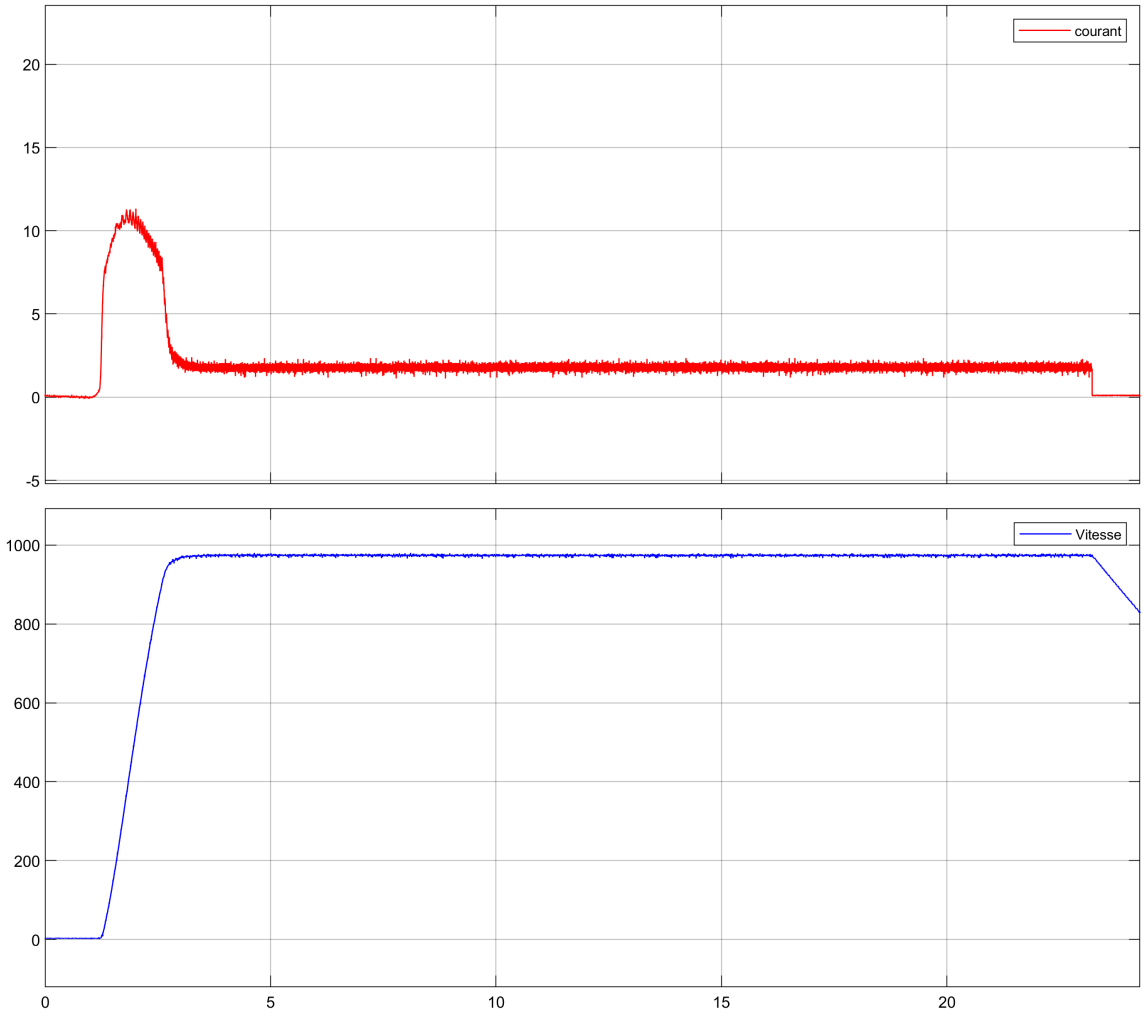

Figure 5: Speed loop — measured response for a $0 \rightarrow 1200$ rpm reference step, showing converter saturation effects.

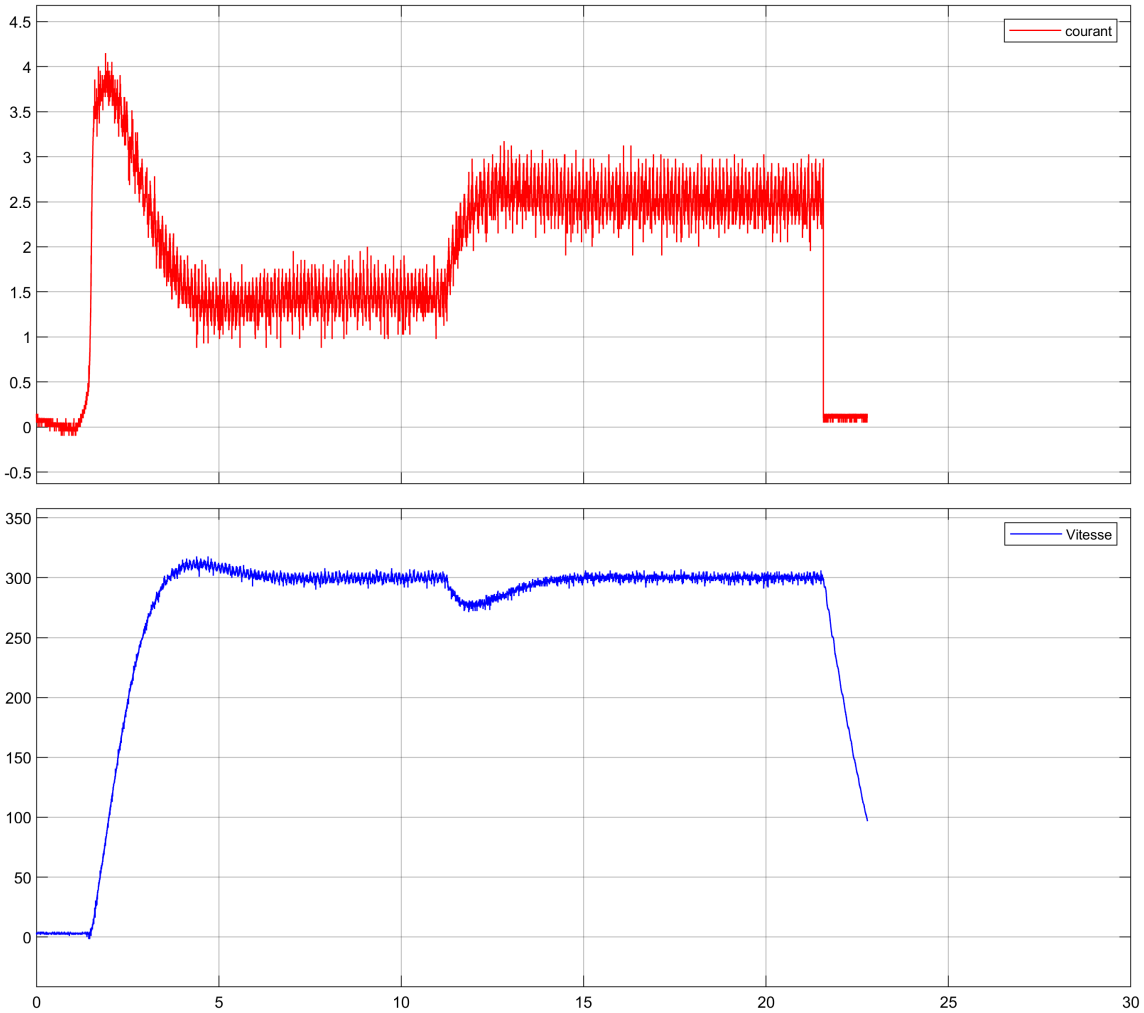

Figure 6: Speed loop — disturbance rejection test: a 5 Nm torque is applied at $t = 10$ s. The controller compensates the perturbation and restores the nominal speed.

3.3 Observer Implementation and Validation

Finally, the observer developed in Section 2.3 was implemented to estimate the states $[\hat{I},\ \hat{\Omega},\ \hat{C}_r]$. The **final Simulink configuration** used for all experiments is shown in Figure 7; it summarizes the complete control architecture (inner current loop, outer speed loop, observer, saturation, and I/O blocks).

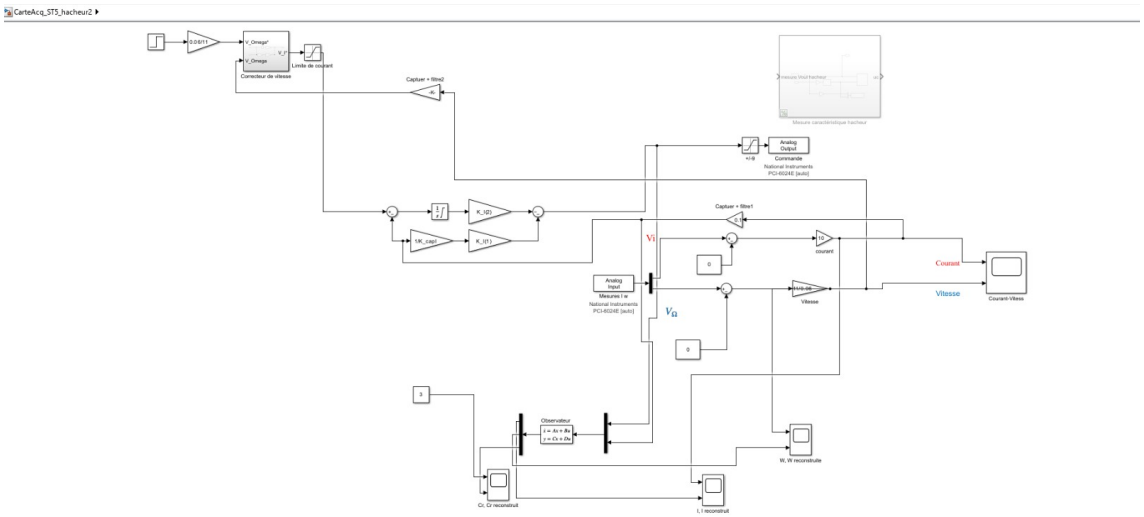

Figure 7: Final Simulink implementation used on the bench (saved during Part 3.3). Earlier configurations for the current and speed loops followed the same structure.

The current estimate converged rapidly and accurately. The speed estimate showed small mismatches and high-frequency noise, mainly due to sensor noise and converter nonlinearities. When using $\hat{C}_r$ for proportional disturbance compensation, the closed loop became sensitive to this noise and could lose stability. Therefore, compensation based on $\hat{C}_r$ was not retained on the bench without additional filtering or gain scheduling. Figure 8 illustrates the convergence of the estimated variables towards their measured counterparts.

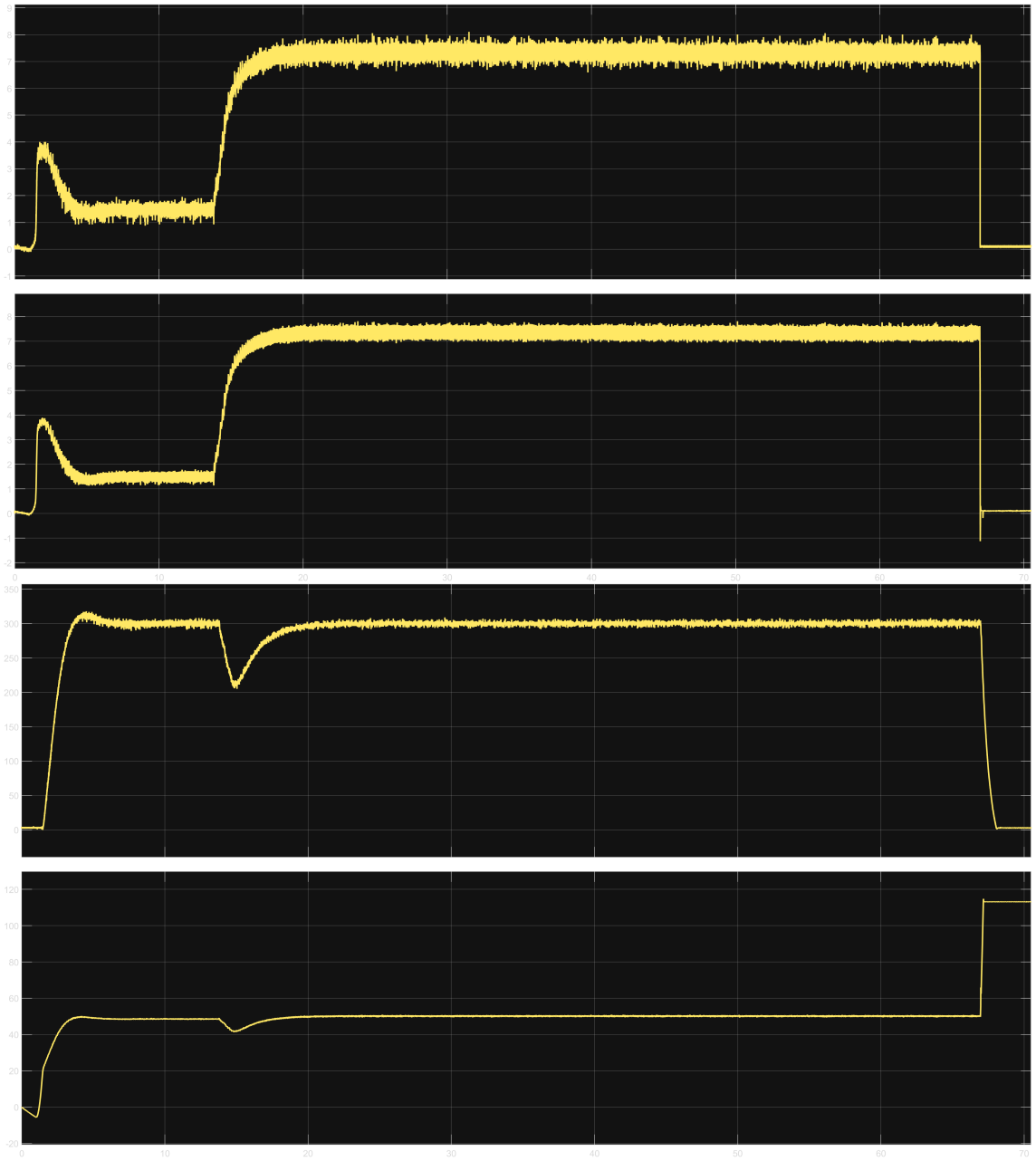

Figure 8: Observer validation — comparison between measured and estimated variables (top: current , bottom: speed).

4 Conclusion

The experimental validation confirmed that the control structures developed in simulation work effectively on the real DC drive, with minor adjustments to account for hardware and safety constraints. The current and speed control loops both met the steady-state and dynamic specifications, demonstrating good robustness against disturbances.

The observer-based approach was successful in simulation and partially in the laboratory. The current estimation was accurate, but the torque estimation was affected by measurement noise, leading to instability when used for disturbance compensation. This highlights the practical challenges of implementing sensorless control on real hardware.

Overall, this practical work successfully connected theoretical modeling, simulation, and experimental implementation. It demonstrated the fundamental principles of cascaded control and observer design, and showed how these techniques can be adapted for real-world electrical drives, where nonlinearity, friction, and converter effects must be carefully handled to ensure system stability and precision.

5 Additional Examples

6 Useful Commands

Here are some useful commands:

Figure 9: Figure caption

Here, I cite the image 9

$$\rho + \Delta = 42 \tag{5}$$

Equation 5 is cited here.